

## Article

# Secure NifTI Image Authentication Scheme for Modern Healthcare System

Kamred Udham Singh <sup>1</sup>, Turki Aljrees <sup>2</sup>, Ankit Kumar <sup>3,\*</sup> and Teekam Singh <sup>4,\*</sup><sup>1</sup> School of Computing, Graphic Era Hill University, Dehradun 248002, India; 11004033@gs.ncku.edu.tw<sup>2</sup> Department College of Computer Science and Engineering, University of Hafr Al-Batin, Hafar Al-Batin 39524, Saudi Arabia; tajrees@uhb.edu.sa<sup>3</sup> Department of Computer Engineering & Applications, GLA University, Mathura 281406, India<sup>4</sup> Department of Computer Science and Engineering, Graphic Era Deemed to be University Dehradun, Uttarakhand 248002, India

\* Correspondence: kumar.ankit@gla.ac.in (A.K.); tsingh@ma.iitr.ac.in (T.S.)

**Abstract:** Advances in digital neuroimaging technologies, i.e., MRI and CT scan technology, have radically changed illness diagnosis in the global healthcare system. Digital imaging technologies produce NifTI images after scanning the patient's body. COVID-19 spared on a worldwide effort to detect the lung infection. CT scans have been performed on billions of COVID-19 patients in recent years, resulting in a massive amount of NifTI images being produced and communicated over the internet for diagnosis. The dissemination of these medical photographs over the internet has resulted in a significant problem for the healthcare system to maintain its integrity, protect its intellectual property rights, and address other ethical considerations. Another significant issue is how radiologists recognize tempered medical images, sometimes leading to the wrong diagnosis. Thus, the healthcare system requires a robust and reliable watermarking method for these images. Several image watermarking approaches for .jpg, .dcm, .png, .bmp, and other image formats have been developed, but no substantial contribution to NifTI images (.nii format) has been made. This research suggests a hybrid watermarking method for NifTI images that employs Slantlet Transform (SLT), Lifting Wavelet Transform (LWT), and Arnold Cat Map. The suggested technique performed well against various attacks. Compared to earlier approaches, the results show that this method is more robust and invisible.



**Citation:** Singh, K.U.; Aljrees, T.; Kumar, A.; Singh, T. Secure NifTI Image Authentication Scheme for Modern Healthcare System. *Appl. Sci.* **2023**, *13*, 5308. <https://doi.org/10.3390/app13095308>

Academic Editor: Mostafa Fouda

Received: 13 March 2023

Revised: 18 April 2023

Accepted: 20 April 2023

Published: 24 April 2023



**Copyright:** © 2023 by the authors. Licensee MDPI, Basel, Switzerland. This article is an open access article distributed under the terms and conditions of the Creative Commons Attribution (CC BY) license (<https://creativecommons.org/licenses/by/4.0/>).

**Keywords:** NifTI; watermarking; medical image; slantlet transform (SLT); lifting wavelet transform (LWT); Arnold cat map

## 1. Introduction

In recent decades, rapid and significant advancements in information technology have increased medical imaging for disease diagnosis. The use of information technology is essential to achieving rapid and accurate outcomes in the field of medical care. The healthcare system utilizes these technologies to expeditiously transfer medical images via the internet for the purposes of diagnosis worldwide. Telemedicine applications, such as teleconsultation, tediagnosis, and telesurgery, are medical procedures requiring the sharing of patient medical information over the internet. A few medical imaging technologies that have significantly contributed to the healthcare system's development are the CT scan, MRI, and Color Doppler. Diagnosis may be made by connecting these medical modalities to radiologists over the internet, generating medical images in various formats viz. DICOM, ANALYZE, NifTI, NRRD, and MINC [1]. Doctors receive diagnosis results that are far faster and much more accurate than film-based imaging methods.

Unlike film-based imaging methods, digital imaging technologies provide a significant benefit in the sense that several radiologists are able to diagnose the same data at the same time from various locations all over the world. Film-based diagnostics have transitioned to

filmless because of expensive printing and transmission expenses. When a patient seeks advice from a doctor, it is beneficial to them [2]. COVID-19 has spread worldwide in recent years, negatively affecting the social lives of billions of people, posing a challenge for researchers to discover a solution by applying medical imaging technology to identify and estimate COVID-19's effect on the lungs. In the present COVID-19 scenario, hospitals have extensive patient data generated through these medical imaging technologies, such as CT scan and MRI image data from patients, communicated through the internet. It is now a frequent practice for various reasons, such as diagnosis, medical consultation, treatment, and remote learning purposes. The communication of these images has been increased recently, but the communication channel is not sufficiently secure. Radiologists and doctors do not take these problems seriously. Therefore, it might be purposefully or unintentionally distorted during the development or transmission of medical images, resulting in catastrophic consequences for patient diagnosis [3]. Therefore, the main concern is the security and authenticity of these medical imaging data from malicious individuals. Thus, the healthcare system requires a solution that addresses this issue of medical images in an unsecured communication network. Watermarking often confirms the image's validity and integrity [4,5]. It is a method that inserts some information in the form of a watermark into the host image without affecting anything about the image, such as the image format or size [6]. If it becomes essential in the future, it will be possible to successfully recover this watermark from the image in order to verify its legitimacy. Faith is lost in the image's legitimacy if any medical image undergoes excessive modification during the watermarking process, and it must hamper the patient's diagnosis. A minor modification in the picture might lead to misdiagnosis, leading to disastrous consequences and legal ramifications. When developing a watermarking scheme for a medical image, remember that it must be reliable and not excessively degrade the image quality.

The use of image encryption in watermarking can provide a powerful combination of security and authenticity, making it an essential technique for protecting and managing digital image data. Encryption can help protect the watermark itself, as it can make it more difficult for attackers to detect and remove the watermark from the image. This can improve the overall robustness and reliability of the watermarking technique, making it more effective for a wide range of applications. Various medical image watermarking encryption techniques have been developed to secure the image via internet communication [7–9].

The two primary classifications utilized to categorize watermarking systems are the transform and spatial domains. The bits of the watermark are incorporated directly into the processes of spatial domain watermarking [10]. However, to begin the process of transform domain watermarking, the host image must first be transformed into the frequency domain utilizing a number of different wavelet transformations, such as DCT, DFT, and DWT. Because robustness is the primary challenge that all digital watermarking techniques face, transform domain methods are more reliable than spatial domain schemes [11,12]. As a consequence of this, the LWT is implemented in the proposed watermarking system.

The majority of researchers have suggested watermarking techniques for medical images in the file formats .jpg, .png, .tiff, and .bmp [13,14], and some have devised watermarking systems for DICOM images (.dcm file extension). Various pioneering medical imaging technologies have been developed in the current medical system. These technologies produce images in the NIFTI format (with an extension of .nii), as opposed to .bmp, .jpg, or DICOM (.dcm file extension). NIFTI images are produced when a lung CT scan is performed on a patient. These images contain extremely sensitive medical data regarding the lungs and are presented in a number of slices. Consequently, the medical system on a global scale requires a reliable watermarking mechanism to validate NIFTI images in advance of diagnosis. Suppose that the watermarking scheme successfully authenticates the medical image (successfully extracting the watermark before starting the diagnosis). In such a scenario, the radiologist will have to decide whether or not to proceed with the diagnosis. Thus, radiologists try to avoid squandering their valuable time on inaccurate medical images for diagnosis. This is accomplished by using the proposed watermarking

method, which could be used in the COVID-19 epidemic to certify these images for proper diagnosis. We first need to identify the appropriate slice from the NIfTI image to begin with this method. Generally, some first and last slices of each NIfTI image contain less medical information, so we select one slice from these slices for watermark insertion. This research is a hybrid watermarking method for NIfTI images that employs the SLT, LWT, and Arnold Cat Map. The proposed scheme is resistant to numerous noise assaults. The following are some of the significant contributions that the proposed watermarking scheme has made:

- A unique watermarking approach for NIfTI images was developed, using LWT, SLT, and BSVD. The combination of LWT and SLT gave more robustness than previous methods.
- The bit error rate was improved by SLT, resulting in a higher percentage of the original energy in the image or signal after compression.
- LL sub-bands have the maximum energy of the signal, so watermark bits were added to the LL sub-band. The combination of SLT and LWT provides more security from several attacks.
- To improve the watermark's level of security, the ACM was utilized to jumble the watermark.

The remaining parts of this paper are divided into the following sections: The methods of image watermarking that are considered to be state of the art are discussed in Section 2; in Section 3, we discuss an overview of the theories that were used in the proposed scheme; in Section 4, we discuss the proposed approach of watermark embedding and extraction process; in Section 5, we conduct simulations and assess the simulation result; and in Section 6, we conclude the study.

## 2. Literature Review

The astonishing improvements in teleradiology have gained the attention of researchers and motivated them to work on the problem of digital medical image authenticity. Essentially, medical pictures are heavily allocated to color and grayscale. However, most of the medical imaging modalities, such as CT scan, MRI, X-Ray, Ultrasound, and so on, typically provide grayscale images in various formats, such as .tiff, .png, .bmp, and .dcm. As a result, researchers are paying increasing attention to medical imaging because of its vast range of applications in the modern medical care framework. Several watermarking systems have been documented in the literature to retain the integrity and validity of these medical images. Hamidi et al. [15] suggested a scheme using discrete Fourier transform and the DCT. They included a jumbled watermark in DCT's middle frequency. The authors also used ACM to encrypt the watermark. The authors tested this scheme with textured and natural images and compared it to other schemes. Khare and Srivastava [16] proposed a new method using Redundant Discrete Wavelet Transform (RDWT), Arnold Transform, and SVD. They applied RDWT, and then the LL sub-band was subjected to a homomorphic transform. Furthermore, the Arnold transform was used to scramble the watermark and insert it into the singular values of SVD. Sun et al. [17] proposed a backpropagation neural network and an Arnold-transform-based scheme. A scrambled watermark bit was inserted into the output of the hidden layer. Zhou et al. [18] suggested a multiple-transformation-based scheme. To strengthen the resilience of this technique, they employed three well-known transforms: DWT, DCT, and discrete fractional random transform. They also used a logistic map and Arnold transform to encrypt the watermark prior to insertion. Chang et al. offered a strategy for embedding a grey watermark into a grey image via a feature classification forest approach [19]. A watermarking approach based on the integer DCT domain was provided for inserting different grey watermarks within host grey images [20]. Kang et al. developed a DWT domain-based technique by combining DCT and SVD and determining the watermark insertion strength using least-square curve fitting [21]. Hsu et al. [22] presented a system for grayscale image processing that utilized DCT and crosses inter-block prediction. Although copyright protection rules are increasingly strict, the grey NIfTI image digital watermarking approach has garnered little attention. Singh et al. [23] investigated a hybrid approach to watermarking that

combined DWT and DCT with SVD matrix decomposition. Additionally, they included the encrypted watermark by using the Arnold Cat Map.

Rayachoti et al. [24] presented a watermarking approach using the Slantlet transform (SLT) and SVD. They began by dividing the entire image into ROI and NROI and selecting the NROI for watermark placement. NROI is further subdivided into  $8 \times 8$  blocks, after which SLT is applied to these blocks, and SVD is applied to the LH sub-band. Finally, the bit of the watermark is embedded in the singular values. Thabit and Khoo [25] described a scheme that performs watermark embedding along with tamper detection and recovery to protect medical information. This scheme used SLT to embed data in ROI and RONI. The IWT coefficient was used to recover information from ROI. The method is resistant to various assaults. Bamel et al. [26] proposed a scheme using the Fast Walsh Transform (FWT), SLT, and SVD. In this scheme, they also used the NROI for watermark insertion. Fast Walsh Transform is applied on the NROI blocks, and then SVD is applied over these blocks to insert the first watermark, and the second watermark was inserted into the image's red channel using SLT transform.

Jayashree and Bhuvaneshwaran [27] demonstrated a hybrid watermarking approach for grayscale images. This technique combines the Z and DWT transformations and the Bidiagonal SVD (BSVD) decomposition. They enhanced the watermark's security by using the Arnold transform. In this particular system, the author began with a DWT that had three levels. The Z transform was then applied to the HL and HH sub-bands that they had selected in the previous step. After that, the Z-transformed component was subjected to BSVD, and the bits of an encrypted watermark were inserted into the S matrix's singular values. Bhatnagar and Raman [28] applied SVD and BSVD to separate images, and inverse SVD and BSVD were used to rebuild them. When the PSNR values acquired by these two approaches are compared, it is evident that the PSNR values obtained by BSVD are greater than those obtained by SVD. Assini et al. [29] proposed a hybrid technique for watermarking. This approach combines the DWT and DCT wavelet transformations with the SVD to break down the components. The medical image is first exposed to three levels of DWT and then to DCT throughout the HH band. The DCT coefficients are then decomposed using SVD, and the singular values are watermarked. Zermi et al. [30] described a method for watermarking medical images based on DWT and SVD. The author created the watermark for this approach by combining patient and image data. The procedure of adding the watermark then commenced. At this stage, the author employed the DWT first, followed by the SVD on the LL sub-band. Finally, the watermark is placed in the singular value matrix's least significant bits. Singh et al. [31] suggested a technique for NIfTI pictures using LWT and QR decomposition, in which the watermark is inserted into the first slice of the image. This approach is good, but the quality of watermark extraction is less resistant to attack.

After thoroughly analyzing the literature and the various contributions, we found that most medical image watermarking approaches are developed for natural images or some for DICOM images. However, there has been no state-of-the-art contribution for NIfTI images. Based on earlier findings, this study proposes an approach for authenticating NIfTI images by combining the Slantlet, lifting wavelet transform, and Arnold Cat Map. Because of their low computational complexity, the LWT and HD were chosen. To successfully include the watermark, the proposed technique employs a hybrid combination of four complicated functions, namely LWT, Slantlet Transform, and ACM. It is a simple approach for scrambling the watermark before insertion, which helps in the security of the watermark. If an unsanctioned person extracts the watermark, they would be unable to deduce anything from it. Watermarking algorithms are open to the public.

### 3. Background Theories

In this section of the paper, we discuss, in detail, the mathematical theories and transformations applied in the design of the watermarking technique.

### 3.1. Slantlet Transform

Ivan (1998) [32] presented SLT as a comparable version of the DWT with better localization and smoothness properties, and it has the ability to control two zeros along with discrete time. A parallel structure is implemented as a solution to the SLT of the filter bank. Instead of filter iteration, it employs various filters for each scale. The length of SLT filters is much shorter as compared to discrete wavelets. The image is transformed by using the column and row transformations. The entire Slantlet Transform is expressed in matrix format as:

$$S = SLT_N s SLT_N^T \tag{1}$$

where  $s$  is the 2D matrix,  $S$  is the Slantlet Transform of the matrix, and  $SLT_N$  is an  $N \times N$  Slantlet matrix. Note that  $s$ ,  $S$ , and  $SLT_N$  must be the same size  $N \times N$ . The matrix multiplication process will be used to obtain the SLT coefficients of the image blocks. In matrix ( $S$ ), the SLT coefficients will be subdivided into four sub-bands, as depicted in Figure 1.

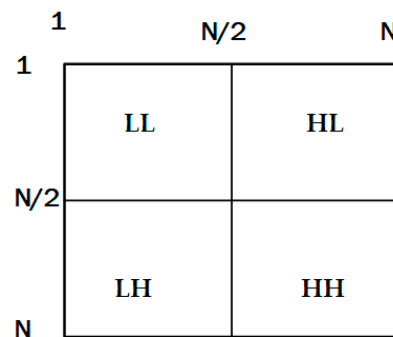


Figure 1. Four sub-bands of SLT coefficients.

Where

$$LL = S \left( 1 : \frac{N}{2}, 1 : \frac{N}{2} \right) \tag{2}$$

$$LH = S \left( \frac{N}{2} + 1 : N, 1 : \frac{N}{2} \right) \tag{3}$$

$$HL = S \left( 1 : \frac{N}{2}, \frac{N}{2} + 1 : N \right) \tag{4}$$

$$HH = S \left( \frac{N}{2} + 1 : N, \frac{N}{2} + 1 : N \right) \tag{5}$$

The inverse SLT transform can be obtained as:

$$s = SLT_N^T S SLT_N \tag{6}$$

### 3.2. Lifting Wavelet Transform

The LWT [33] preserves the transform domain, which is consistently applied in an integer-to-integer method. In LWT, the image is composed of four bands, labeled from lowest to highest intensity: LL, LH, HL, and HH. The low-frequency components include significantly higher energy in the image than the high-frequency components. The construction of a signal may be broken down into three stages in the lifting method as follows [34]:

- Split—During this phase, the signal  $\omega(n)$  is divided into odd and even ( $\omega_o(n), \omega_e(n)$ , respectively) sets as:

$$\omega_e(n) = \omega(2n), \omega_o(n) = \omega(2n + 1) \tag{7}$$

- Predict—It is assumed that an odd set will result from an even set at this stage. In the high pass, the predict phase is responsible for compensating for the occurring polynomial components. Consequently, another name for this phase is the high-pass filtering step of the procedure. Therefore, the difference  $\varphi(n)$  is

$$\varphi(n) = \omega_o(n) - P_r[\omega_e(n)], \tag{8}$$

$P_r [.]$  stands for the predict operator in this equation, and  $(n)$  represents a high-frequency component. The value of  $\varphi(n)$  represents the deviation between the original set and the projected value.

- Update—This is to determine that the scaling function even set  $\omega_e(n)$  is updated by the wavelet coefficient. Moments from the low pass are also retained in this step of the process. It is defined as

$$L(n) = \omega_e(n) + U_p[\varphi(n)] \tag{9}$$

### 3.3. Bidiagonal Singular Value Decomposition (BSVD)

SVD matrix decomposition decomposes the matrix into the diagonal and orthogonal matrix as follows

$$A = USV^T \tag{10}$$

BSVD is calculated using finite operations, whereas SVD requires iterative techniques to determine singular values [35]. As demonstrated below, the BSVD is calculated by bidiagonalizing  $X$  and then performing SVD on the top bidiagonal values:

$$X = U_X W V_X^T \tag{11}$$

$A$  is a matrix that decomposes into three components  $U_X$ ,  $W$ , and  $U_A$ , where  $U_X$  is an orthonormal matrix,  $U_A$  is a unitary matrix, and  $W$  is strictly an upper bidiagonal matrix. Then, SVD is applied on the  $W$  as follows

$$W = U_W S V_W^T \tag{12}$$

where  $U_W$  and  $V_W$  are both the unitary matrix, and  $S$  is the singular value matrix. Thus, the BSVD of matrix  $X$  can be achieved by using Equations (11) and (12) as follows

$$X = U_X U_W S V_W^T V_X^T \tag{13}$$

### 3.4. Arnold Cat Map

This alters the original placements of the pixels in the image at random; we use it for watermark encryption. Because of its simplicity, periodicity, and reversibility, this 2D mapping approach is used in encryption and watermarking [36]. A transform’s periodicity and reversibility suggest that the original data will be recovered after a fixed iteration if applied repeatedly to a given matrix. ACM can be expressed as follows:

$$\begin{bmatrix} i' \\ j' \end{bmatrix} = \begin{bmatrix} 1 & r \\ p & rp + 1 \end{bmatrix} \begin{bmatrix} i \\ j \end{bmatrix} \text{mod } Z \tag{14}$$

where  $Z$  defines the size of the host image;  $i$  and  $j \in \{0, 1, 2, \dots, N - 1\}$  are a set of control parameters used to increase security while selecting the mapping frequency.

ACM merely modifies the image data and does not affect the image’s intensity. The relationship between neighboring pixels is entirely shattered after numerous transformations. ACM uses a substantial gain factor to ensure that the alterations brought about by watermark embedding are evenly distributed throughout the image, making it visually unnoticeable in addition to the security advantage.

#### 4. Proposed Watermarking Method

This section begins by introducing the procedures that are recommended for watermark embedding and then moves on to discuss the methods that have been proposed for watermark extraction. The reversible phases of the watermark embedding process are the ones that make up the watermark extraction process.

##### 4.1. Watermark Embedding Process

In this process, first, the patient's information is separated from the NIfTI image and preserved securely. Then, the focus is on selecting the appropriate slice from the NIfTI image for watermark embedding because it has the number of slices. Generally, some slices at the beginning and end contain less information, so we select the slice from these. The selected slice is subjected to LWT; then, the LL sub-band is transformed by ST, separating it into low- and high-frequency bands (LL, HL, HH, LH). The BSVD algorithm decomposes the LL band, and, after that, the encrypted watermark is embedded into the bidiagonal singular values. We use the ACM for watermark encryption, which provides more robustness. In the last step, the watermarked slices, other slices, and the information on the patient are integrated to produce the watermarked NIfTI image. The procedures required for embedding a watermark are detailed below Algorithm 1:

---

##### Algorithm 1 Watermark Embedding Process

---

**Input:** NIfTI Image  $\mathcal{M}$  ( $630 \times 630$ ) || Watermark  $\mathbb{I}$  ( $128 \times 128$ )

**Output:** Watermarked NIfTI image

**Step 1.** Segregate meta information and select the slice  $S$  as per the above discussion from the image.

**Step 2.** Perform one-level LWT on the original image  $S$

$$\text{LWT}(S) = [\text{LH}, \text{HL}, \text{LL}, \text{HH}] \quad (15)$$

**Step 3.** Using Equation (1), apply SLT on the LL band.

$$\text{SLT}[\text{LL}] = [\text{LH}, \text{HL}, \text{LL}, \text{HH}] \quad (16)$$

**Step 4.** Apply the BSVD on the LL band using Equation (13), so we obtain five matrixes  $U_X$ ,  $U_W$ ,  $S$ ,  $V_W^T$ , and  $V_X^T$ , where the  $S$  matrix is the bidiagonal singular matrix of the slice.

$$\text{BSVD}(\text{LL}) = U_X \times U_W \times S \times V_W^T \times V_X^T \quad (17)$$

**Step 5.** Perform ACM on the watermark using the key using Equation (14).

$$\mathcal{K} = \text{ACM}(\mathbb{I}) \quad (18)$$

**Step 6.** Encrypted watermark's bits are embedded in the singular values of matrix  $S$  as

$$S + \rho\mathcal{K} = U_{\mathcal{K}} \times S_{\mathcal{K}} \times V_{\mathcal{K}}^T \quad (19)$$

where  $\rho$  is the embedding strength.

**Step 7.** The modified LL band of the SLT transform is evaluated as in Equation (20).

$$\text{LL}_{\text{mod}} = U_X \times U_W \times S_{\mathcal{K}} \times V_W^T \times V_X^T \quad (20)$$

**Step 8.** Perform inverse SLT transform using  $\text{LL}_{\text{mod}}$  as the following equation

$$\text{LL}' = \text{ISLT}[\text{LL}_{\text{mod}}, \text{LH}, \text{HL}, \text{HH}] \quad (21)$$

**Step 9.** To create the final watermarked slice  $S'$ , conduct inverse LWT:

$$S' = \text{ILWT}[\text{LL}', \text{LH}, \text{HL}, \text{HH}] \quad (22)$$

**Step 10.** To generate the final watermarked NIfTI image  $M'$ , we combine the patient's metadata and other slices with the watermarked slice.

---

The above-discussed watermarking steps can be applied to any slice of the NIfTI image for watermark embedding. If someone is more worried about security, they can insert the watermark into multiple slices of the NIfTI image. As we know, the NIfTI images are an array of slices where some slices at the beginning and end have less medical information. Therefore, the selection from these slices never hampers the patient's diagnosis, but if in-between slices are used for watermark insertion, an incorrect diagnosis may be reached. However, we used these slices for the experiment to prove the superiority of the proposed watermarking approach. Figure 2 provides a graphical representation of the whole process of embedding a watermark in an NIfTI image.

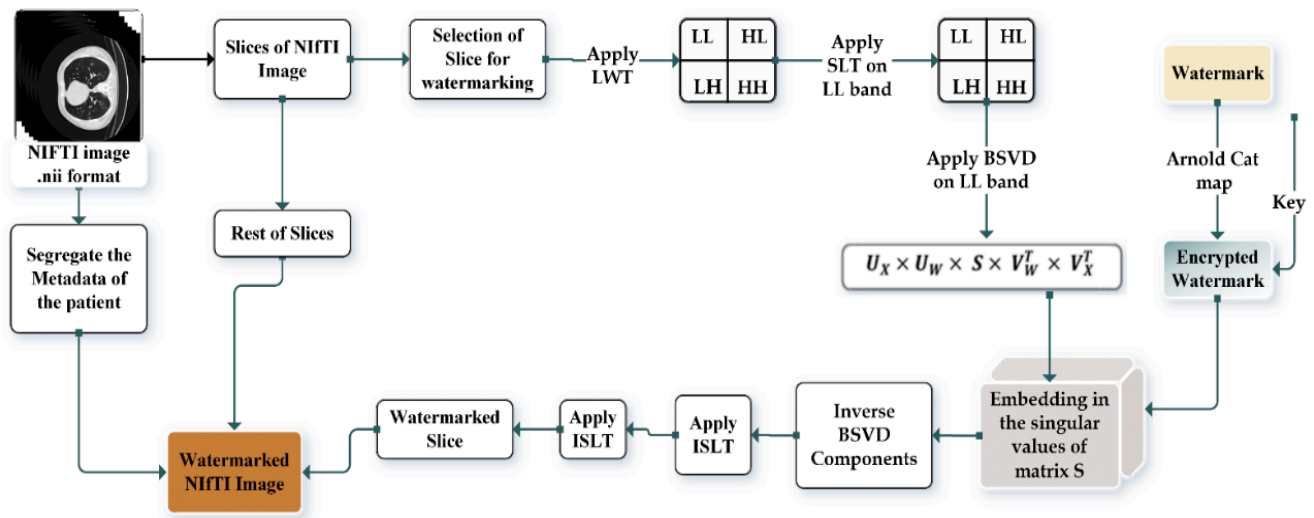


Figure 2. Complete procedure of watermark embedding.

4.2. Watermark Extraction Process

The extraction of watermarks is a fundamental process in every watermarking system. Initially, the patient’s metadata are segregated from the image, and then the watermarked slice is selected from the watermarked NIFTI image. The LWT is then applied to the selected slices, resulting in the slices being divided into various frequency sub-bands. The SLT is then applied to the LL band, and the BSVD immediately follows it. In the last step, the ACM algorithm is applied to the bits recovered from the singular matrix to create the watermark. The proposed watermark extraction approach is described in Figure 3 and the Algorithm 2 is as follows

Algorithm 2 Watermark Extraction Process

**Input:** Watermarked NIFTI image  $\mathcal{M}'$

**Output:** Extracted watermark

**Step 1.** Select the watermarked slice  $\mathcal{M}'$ .

**Step 2.** Perform one-level LWT on the watermarked slice  $\mathcal{M}'$

$$LWT(\mathcal{M}') = [LH', HL', LL', HH'] \tag{23}$$

**Step 3.** Apply SLT on the LL band using Equation (1).

$$SLT[LL'] = [LH^*, HL^*, LL^*, HH^*] \tag{24}$$

**Step 4.** Apply the BSVD on the LL band using Equation (13) and obtain

$U'_X, U'_W, S', V'^T_W$ , and  $V'^T_X$ , where S matrix is the bidiagonal singular matrix of the slice.

$$BSVD(LL^*) = U'_X \times U'_W \times S' \times V'^T_W \times V'^T_X \tag{25}$$

**Step 5.** Calculate the  $D'$  using the following equation

$$D' = U'_K \times S'_K \times V'^T_K \tag{26}$$

**Step 6.** Extraction of watermark’s bits is computed as the reversing formula of embedding, as given in the following equation

$$B = (D' - S') / \rho \tag{27}$$

**Step 7.** Finally, decrypt the watermarking using the inverse ACM on the extracted bits using the key to generate the watermark.

$$I' = IACM(B) \tag{28}$$

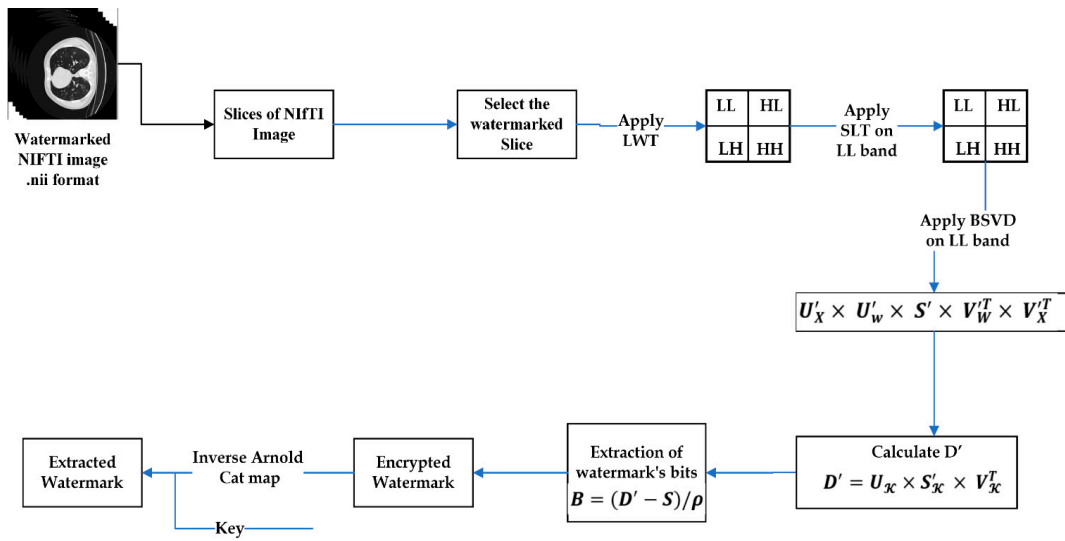


Figure 3. Watermark extraction process.

### 5. Experimental Results and Discussion

The proposed watermarking approach is evaluated using the NifTI slice generated from a CT scan of a COVID-19 patient [37]. We are following the ethical standards of medical practice by not disclosing the patient’s identity. The simulation was run on a MATLAB 2022a platform, and the machine used to run it had an Intel i7-10750 CPU running at 2.6 GHz with six cores, a Windows 10 operating system, and 8 gigabytes of RAM. The experiment employed ten NifTI images with a slice size of  $630 \times 630$  pixels and a .bmp grayscale watermark of  $128 \times 128$ . The number of slices in each NifTI image is depicted in Figure 4. Each NifTI image may have a varied number of slices. Figure 5 depicts all of the NifTI\_3 image slices. Figure 5 clearly indicates that, as previously discussed, some starting and ending slices provide less medical information; we use the less-informative slice for watermark insertion.

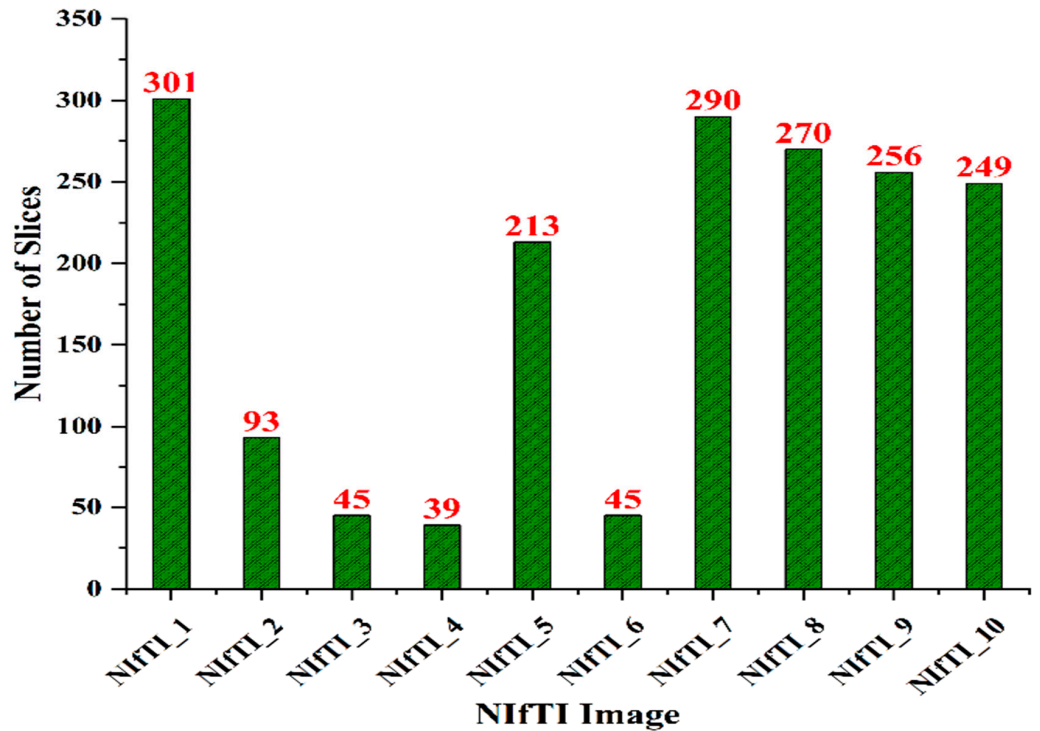


Figure 4. Number of Slices in NifTI images used for the proposed scheme.

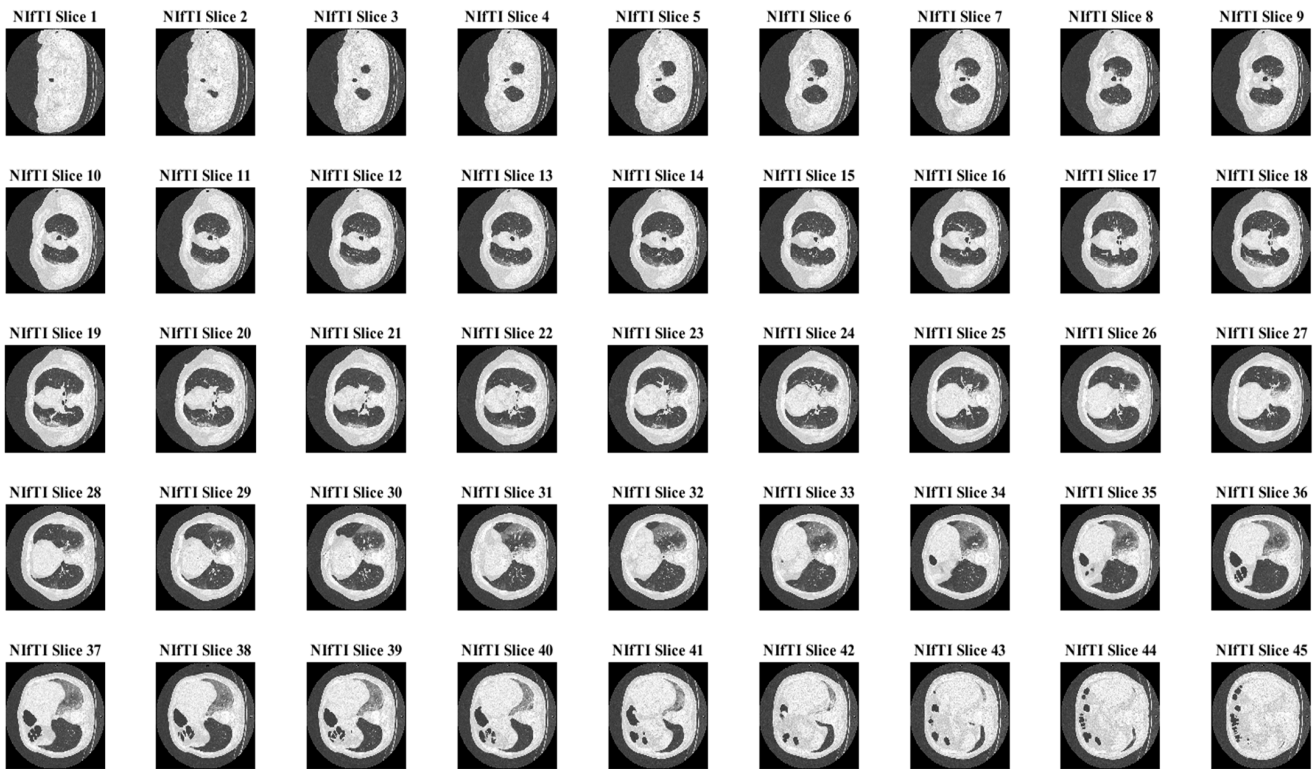


Figure 5. All slices in one Nifti image.

5.1. Performance Evaluation Metrics

The suggested watermarking method is assessed by using the Peak Signal to Noise Ratio (PSNR), Image Quality Index Q, Structural Similarity Index Measure (SSIM), and Normalized Correlation (NC) [38]. PSNR, Q, and SSIM are the metrics applied to evaluate the influence that various parameters of the proposed method have on the imperceptibility of the watermarked slice. The PSNR evaluation formula is given in Equation (30). PSNR is affected by the Mean Square Error.

$$PSNR = 10 * \log_{10} \frac{(Max)^2}{\frac{1}{m*n} \sum_{i=0}^m \sum_{j=0}^n (A_{ij} - B_{ij})^2} \tag{29}$$

To evaluate how similar the original slice and the watermarked slice are to one another, the SSIM is used. The value of the SSIM can vary from  $-1$  to  $+1$ ; if SSIM is equal to  $1$ , then the original slice and the watermarked slice are the same. The SSIM is computed using Equation (30)

$$SSIM(x, y) = \frac{(2\mu_x\mu_y + c_1) (2\sigma_{xy} + c_2)}{(\mu_x^2 + \mu_y^2 + c_1) (\sigma_x^2 + \sigma_y^2 + c_2)} \tag{30}$$

where  $\mu_x$  and  $\mu_y$  represent the mean values of the original image and the watermarked image, respectively;  $\sigma_x^2$  and  $\sigma_y^2$  represent the variances in the original image and the watermarked image, respectively.  $\sigma_{xy}$  is the covariance.

Estimating the degree of similarity between the host slice and the generated watermarked slice is necessary to evaluate how resistant the proposed method is. This is performed with the help of the NC parameter. If the NC value is quite near to one, the solution provided is effective in terms of recovery strength. NC computation is given as Equation (31).

$$NC = \frac{\sum_{x=1}^M \sum_{y=1}^N w(x, y) \times w^*(x, y)}{\sum_{x=1}^M \sum_{y=1}^N w^2(x, y)} \tag{31}$$

The following is a definition of the universal image quality index Q:

$$Q = \frac{4\sigma_{xy}\bar{x}\bar{y}}{(\sigma_x^2 + \sigma_y^2)[(\bar{x})^2 + (\bar{y})^2]} \quad (32)$$

### 5.2. Result Analysis

Experiments were carried out to investigate the fundamental prerequisites of the proposed watermarking scheme: visual quality of watermarked image, security, integrity, confidentiality, invisibility, and robustness. The ability to hide the watermark in an image without affecting its visual quality is referred to as invisibility. PSNR is a critical statistic for determining invisibility. The performance of the proposed approach is tested on 10 diverse NIfTI images, and the slices used for the watermark insertion and extraction process are Slc1 to Slc10. The results showed that our approach was imperceptible and resilient. The pixel size of the slices is  $630 \times 630$  pixels, while the watermark size is set at  $128 \times 128$  pixels, as shown in Figure 6.

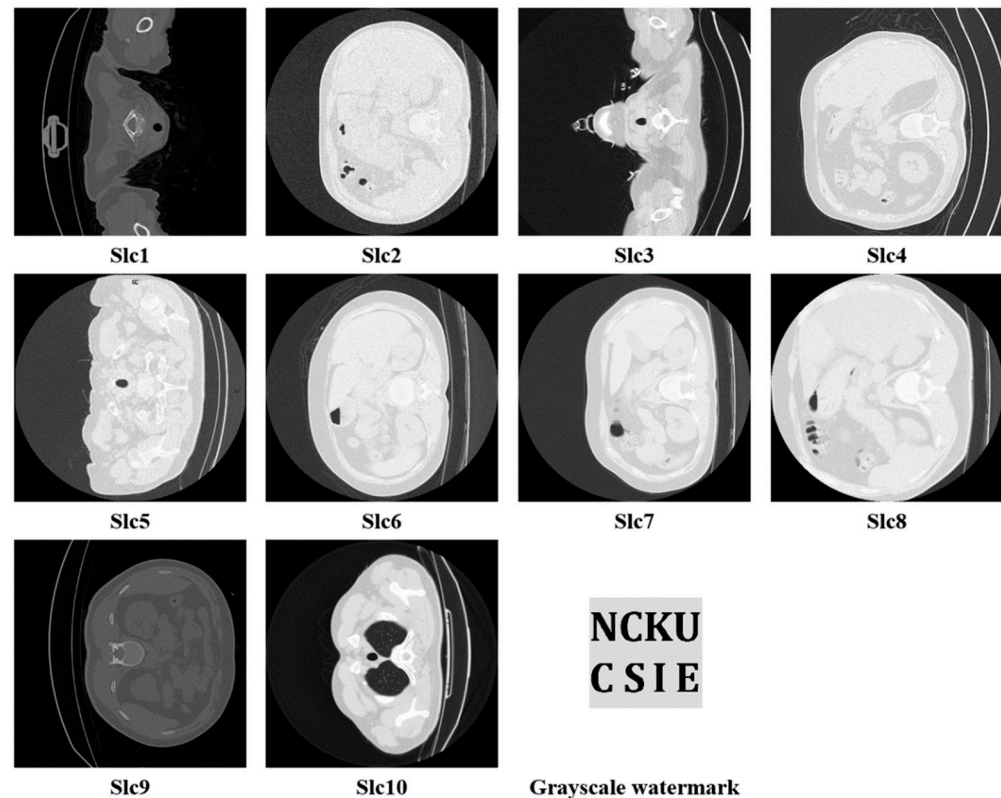


**Figure 6.** Slices of NIfTI image (Slc1 to Slc10) used for experimental analysis.

Our approach's performance was evaluated using a selected slice of the NIfTI images. Table 1 displays the image quality evaluation parameters of the watermarking system as well as the extracted watermark. If Q, NC, and SSIM are close to one, this signifies that the original and watermarked slices are essentially identical. The slice that is watermarked has a PSNR that is higher than 53 dB, indicating that the watermarked image is of exceptionally high quality. The extracted watermark quality from all the slices is significant, proving that our proposed scheme is suited for the watermarking of NIfTI images.

**Table 1.** Major quality metrics of the proposed watermarking scheme.

Slices of NIFTI Image	NC	Q	PSNR	SSIM	Extracted Watermark
Slc1	0.9997	0.9996	54.31	0.9894	<b>NCKU CSIE</b>
Slc2	0.9994	0.9995	53.82	0.9947	<b>NCKU CSIE</b>
Slc3	1	0.9999	53.96	0.9912	<b>NCKU CSIE</b>
Slc4	0.9989	0.9991	53.75	0.9928	<b>NCKU CSIE</b>
Slc5	1	0.9999	54.16	0.9899	<b>NCKU CSIE</b>
Slc6	0.9996	0.9993	53.21	0.9965	<b>NCKU CSIE</b>
Slc7	1	0.9998	53.86	0.9936	<b>NCKU CSIE</b>
Slc8	1	0.9997	54.21	0.9898	<b>NCKU CSIE</b>
Slc9	0.9997	0.9990	53.67	0.9890	<b>NCKU CSIE</b>
Slc10	1	0.9998	53.88	0.9939	<b>NCKU CSIE</b>

Once the watermark has been appropriately extracted from the supplied NIfTI image, radiologists or other medical practitioners are responsible for ensuring that they diagnose the ideal medical image. It is a question of life and death for the sufferer. A patient’s unique ID and name might be included as a watermark in the form of a logo or image. Thus, we believe that our technique will play a critical role in verifying NIfTI images. Figure 7 shows the significant parameters of the generated watermarked image in the proposed scheme. We depict the NC, Q, PSNR, and SSIM of the watermarked slice in Figure 7. The proposed scheme’s results are promising, where SSIM, Q, and NC of the proposed approach are near one, and the PSNR is around 54 db.

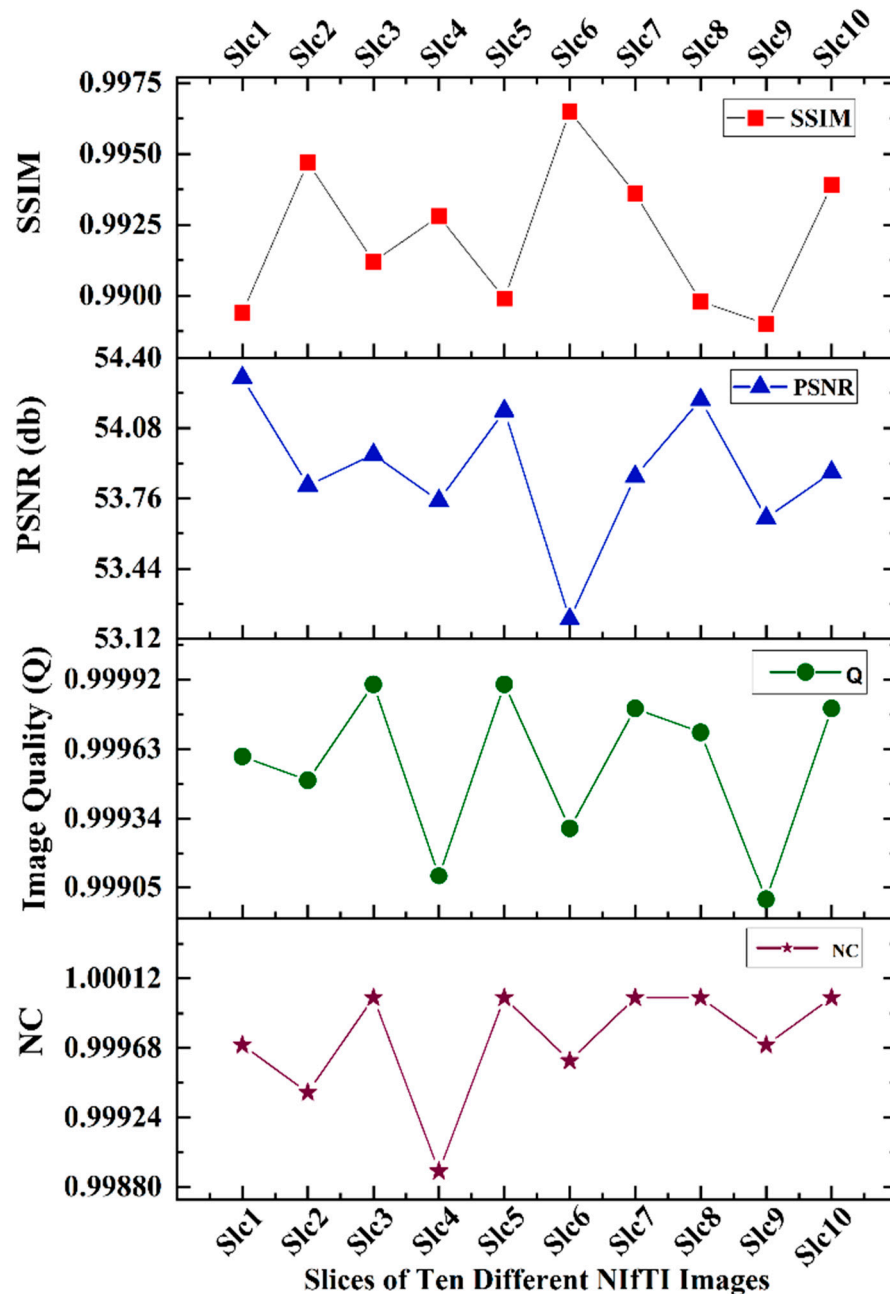
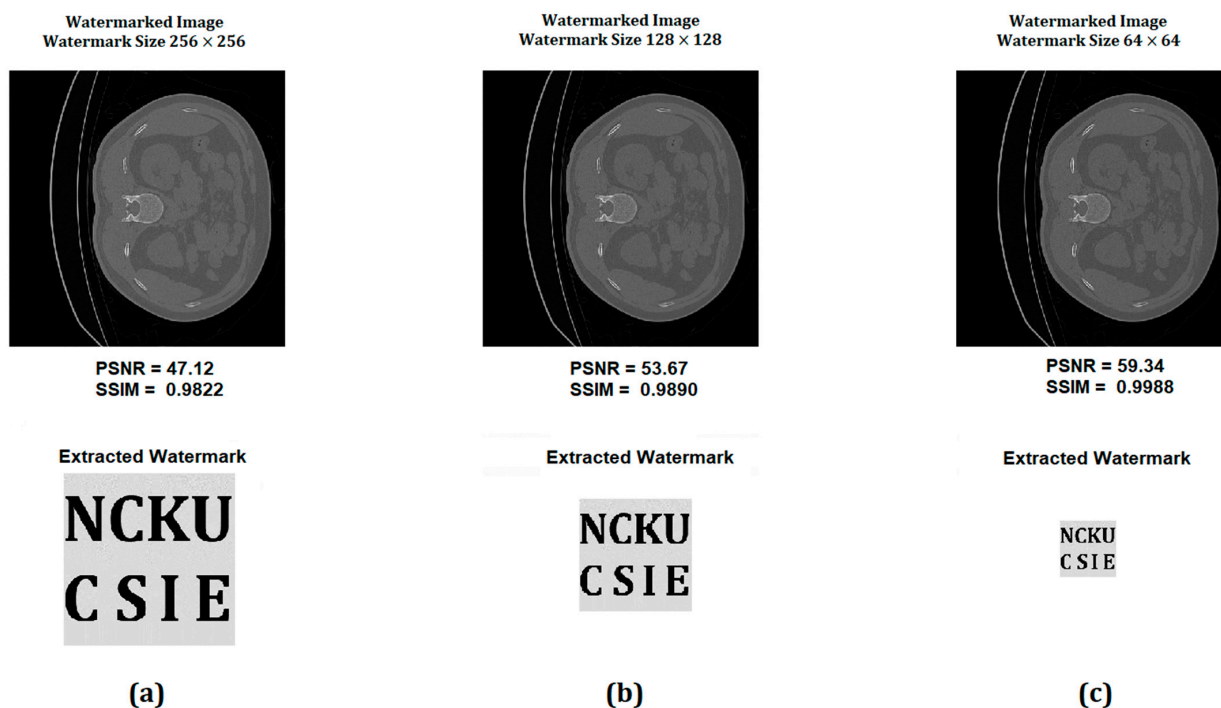


Figure 7. NC, Q, PSNR, and SSIM of the watermarked slice in the proposed watermarking scheme.

The proposed scheme is also evaluated with the different sizes of watermark embedding. For the experiment, we embedded the watermark at sizes of  $64 \times 64$ ,  $128 \times 128$ , and  $256 \times 256$  in the slice. Figure 8a displays the watermarked slice and the  $256 \times 256$  watermark recovered from the particular slice, where the PSNR of the watermarked image

is 47.12 db and the SSIM is 0.9822. Figure 8b shows the watermarked slice as well as the extracted watermark at a size of  $128 \times 128$ , where the PSNR is 53.67 and the SSIM is 0.989. Figure 8c shows the watermarked slice and extracted watermark at a size of  $64 \times 64$ , where the PSNR is 59.34 and the SSIM is 0.9988. If the large-scale watermark is embedded, it degrades the quality of the watermarked slice. Thus, it is essential to utilize a small-sized watermark for medical image authentication purposes.



**Figure 8.** Different sizes of watermark embedding and extraction without any attack. (a) Embedding and Extraction Results on the embedded watermark size  $256 \times 256$ . (b) Embedding and Extraction Results on the embedded watermark size  $128 \times 128$ . (c) Embedding and Extraction results on the embedded watermark size  $64 \times 64$ .

### 5.3. Comparison with Existing Schemes

In this part, the performance of the proposed approach is compared to that of current watermarking methods. Based on these comparisons, it is clear that the proposed approach was highly successful in producing a watermarked image of good quality. Furthermore, the comparison is carried out by inserting a  $128 \times 128$ -pixel watermark into a  $630 \times 630$ -pixel NIfTI image slice. The results of our suggested methodology are compared in Table 2 with the results of other techniques that are currently accessible. The comparison reveals that the results obtained using our procedure were far more substantial than those obtained using existing strategies. As shown in Table 2, in terms of PSNR, our technique outperformed the methods of Kumar et al. [1], Singh et al. [2], Sun et al. [17], Kang et al. [21], Rayachoti et al. [24], Rasha et al. [25], and Bamal et al. [26] and also showed significant PSNRs. Our approach's SSIM is closer to one than other existing techniques, demonstrating the improved quality of the watermarked slice produced by our methodology. Figure 9 visually represents an NC comparison between the proposed system and three other current methods. viz. Kumar et al. [1], Singh et al. [2], and Sun et al. [17]. In some cases, our method approaches the maximum normalized correlation. In some cases, however, it is closer to the benchmark. The average NC is 0.99973. The comparison between the NC of the proposed system and that of Kumar et al. [1], Singh et al. [2], and Sun et al. [17] is seen rather well on the graph. The NC of the proposed approach is closer to one compared to the NC of any other technique, which means the quality of the watermarked picture produced by the proposed method is superior to that produced by any other method.

**Table 2.** PSNR, SSIM, and NC compared to other existing methods.

Image	Proposed Scheme			Kumar et al. [1]		Singh et al. [2]		Sun et al. [17]		Kang et al. [21]		Rayachoti et al. [24]		Rasha et al. [25]	Bamal et al. [26]	
	SSIM	NC	PSNR	PSNR	NC	SSIM	PSNR	NC	PSNR	NC	PSNR	SSIM	PSNR	SSIM	PSNR	PSNR
Slc1	0.9894	0.9997	54.31	41.89	0.9975	0.9474	46.98	0.998893	44.2034	0.9982	38.71	0.9714	52.36	0.9938	42.2544	53.8014
Slc2	0.9947	0.9994	53.82	41.9	0.9968	0.947	46.38	0.999184	51.6799	1	40.07	0.972	51.36	0.9906	42.0782	54.0554
Slc3	0.9912	1	53.96	41.86	0.9977	0.9599	46.94	0.998919	35.7588	0.9948	36.48	0.9585	50.27	0.9891	40.5454	54.5383
Slc4	0.9928	0.9989	53.75	41.87	0.9969	0.9469	46.88	0.998744	35.4769	0.9793	37.14	0.9795	54.09	0.9929	32.5856	53.7501
Slc5	0.9899	1	54.16	41.85	0.9976	0.948	46.92	0.998716	48.7506	0.9991	42.25	0.9747			42.4724	53.8454
Slc6	0.9965	0.9996	53.21	41.91	0.9976	0.9475	46.91	0.998719	44.7388	0.9903	39.38	0.9572			39.4181	52.8659
Slc7	0.9936	1	53.86								39.1	0.9613				49.6742
Slc8	0.9898	1	54.21								35.9	0.955				53.6426
Slc9	0.989	0.9997	53.67													
Slc10	0.9939	1	53.88													
Average	0.9921	0.9997	53.88	41.88	0.9974	0.9495	46.84	0.99886	43.4347	0.9936	38.6288	0.9662	52.02	0.9916	39.8924	53.2717

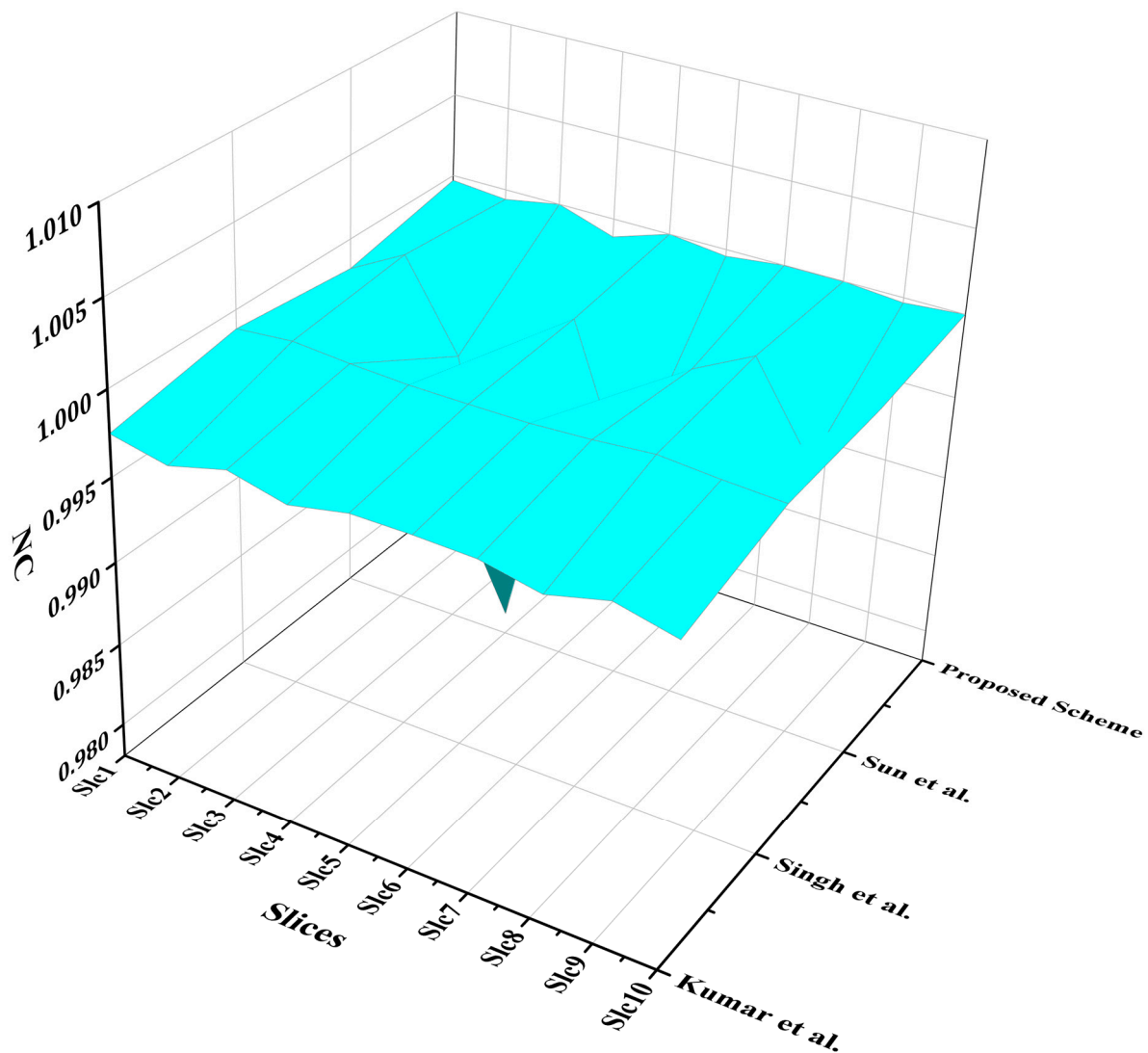


**Figure 9.** NC of the proposed scheme vs. the existing schemes Kumar et al. [1], Singh et al. [2], Sun et al. [17].

The PSNR of the watermarked image is a significant parameter to evaluate the quality of any watermarking system. The average PSNR of our scheme is 53.89 db, whereas the average PSNR of other schemes such as Kumar et al. [1] is 41.88 db, Singh et al. [2] is 46.84 db, Sun et al. [17] is 43.4347 db, Kang et al. [21] is 38.6288 db, Rayachoti et al. [24] is 52.02 db, Rasha et al. [25] is 39.8924 db, and Bamal et al. [26] is 53.2716 db as depicted in Figure 10. Only the PSNR of Bamal et al. [26] is closer to the proposed scheme; otherwise, they lie between 38 db and 52 db. Figure 11 shows another important quality evaluation parameter of the watermarked scheme, i.e., SSIM. This graph illustrates a comparison of the proposed approach with the three previously presented approaches viz. Rayachoti et al. [24], Kumar et al. [1], and Kang et al. [21].

In the sequence of comparison scenario, the next parameter compared the SSIM shown in Figure 11. The proposed scheme is compared with Kumar et al. [1], Kang et al. [21], and Rayachoti et al. [24], and we found that the average SSIM of the proposed scheme is 0.99208, whereas, for Kumar et al. [1], Kang et al. [21], and Rayachoti et al. [24], it is 0.94945, 0.9662, and 0.9916, respectively, indicating that the proposed scheme improved the quality of the watermarking scheme. In summary, the proposed scheme improved the visual quality of watermarked images compared to other existing watermarking schemes.

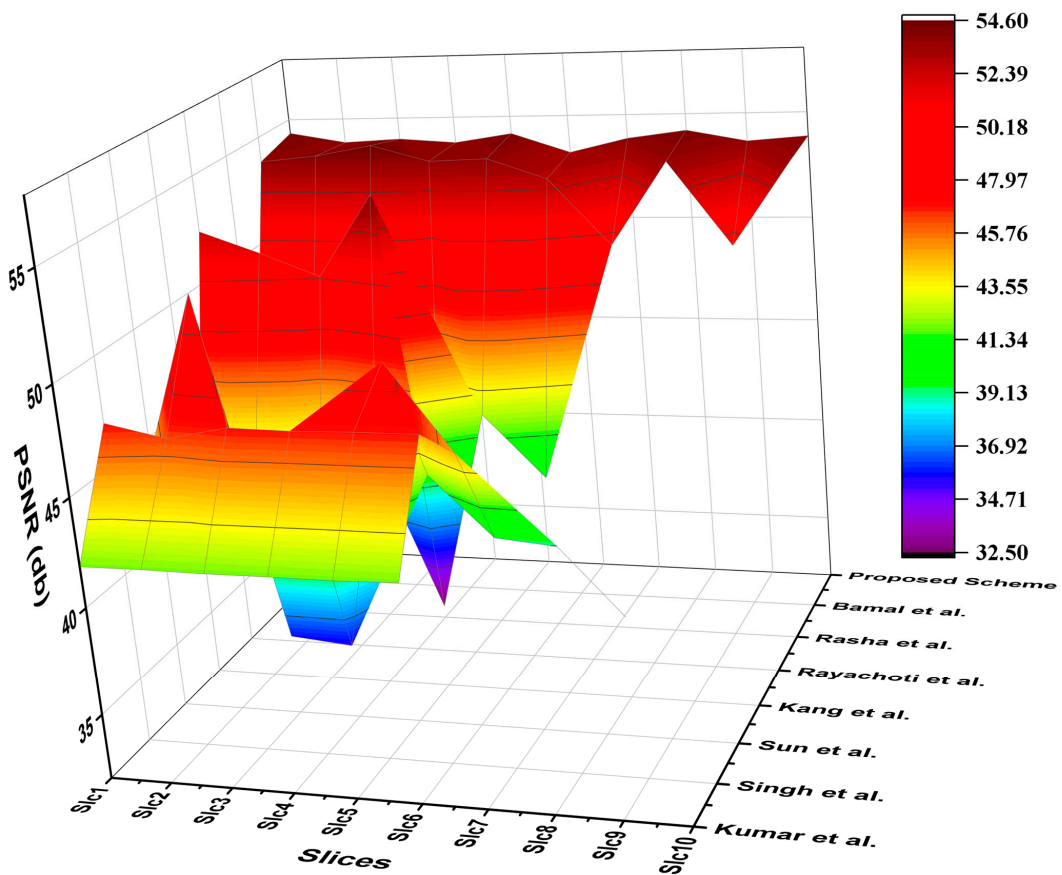


Figure 10. PSNR of the proposed system vs. the existing schemes Kumar et al. [1], Singh et al. [2], Sun et al. [17], Kang et al. [21], Rayachoti et al. [24], Rasha et al. [25], Bamal et al. [26].

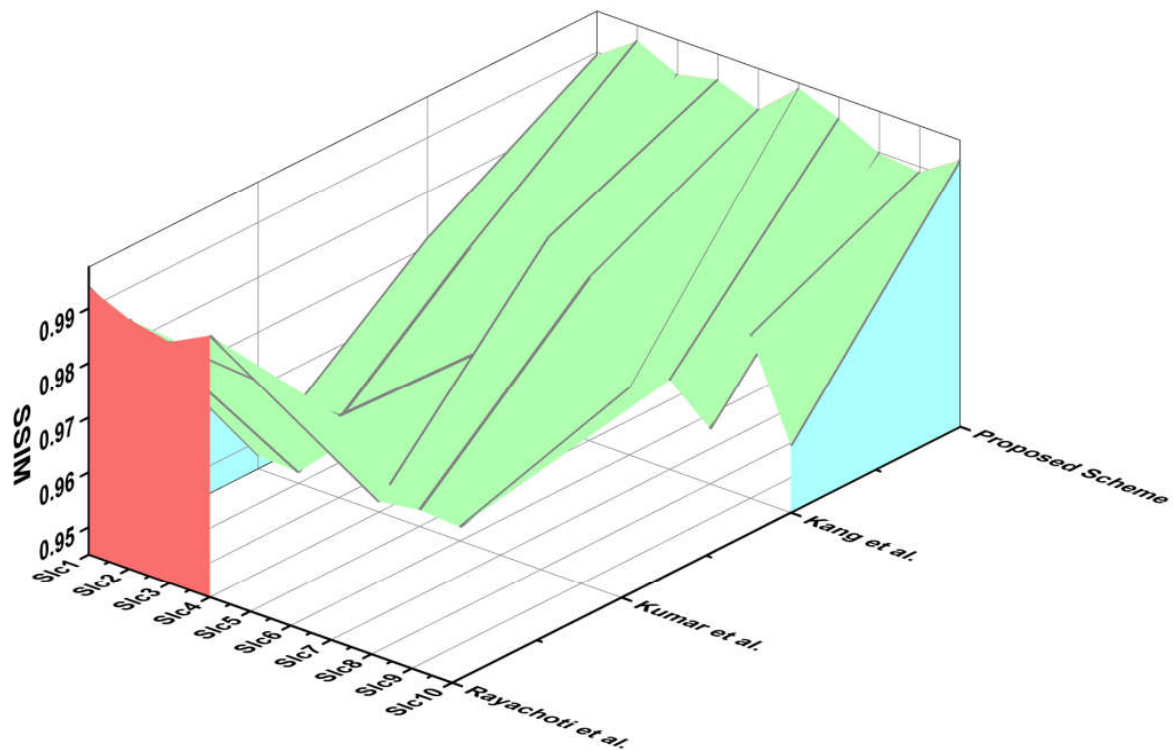


Figure 11. SSIM of the proposed system vs. the existing schemes Kang et al. [21], Kumar et al. [1], Rayachoti et al. [24].

Table 3 shows a comparison of the average value of PSNR, NC, and SSIM in the proposed work and with the existing methods. It shows that the proposed scheme has more significant results than the other models.

**Table 3.** Comparative analysis of average PSNR, NC, and SSIM with proposed work vs. the existing method.

Author	PSNR	NC	SSIM
Kumar et al. [1] (2022)	41.88	0.9974	0.9495
Singh et al. [2] (2022)	46.84	0.99886	-
Sun et al. [17] (2018)	43.4347	0.9936	-
Kang et al. [21] (2018)	38.6288	0.9662	-
Rayachoti et al. [24] (2017)	52.02	-	0.9916
Rasha et al. [25] (2017)	39.8924	-	-
Bamal et al. [26] (2019)	53.2717	-	-
Proposed Scheme	53.88	0.9997	0.9921

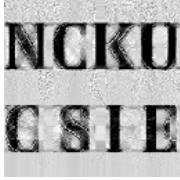
#### 5.4. Robustness Analysis

The above findings show that our technique provided substantial results on various slices of distinct NIfTI images. Our technique's resilience is verified against various image processing threats. We compromised with the watermarked slice by adding several types of noise, such as salt-and-pepper noise, Poisson noise, compression, Gaussian noise, speckle noise, motion blur, etc. Watermarks are extracted after attacks, and the NC values of extracted watermarks are shown in Table 4 against unintentional attacks. The retrieved watermarks' quality was reduced but still adequate under specific attacks.

**Table 4.** Watermarks extracted under various attacks.

Name of Attack	Extracted Watermark	NC of Extracted Watermark
Salt and pepper noise (0.001)		0.9491
Salt and pepper noise (0.003)		0.9234
Salt and pepper noise (0.005)		0.8736

Table 4. Cont.

Name of Attack	Extracted Watermark	NC of Extracted Watermark
Gaussian low-pass filter ( $4 \times 4$ )		0.9534
Median ( $4 \times 4$ )		0.9479
Histogram equalization		0.9152
Average filter ( $4 \times 4$ )		0.9425
Gaussian noise (0.002)		0.9482
JPEG 70 compression		0.9564
Sharpening (0.2)		0.9347
Motion blur (0.2)		0.8456

## 6. Conclusions

In this paper, a unique watermarking approach for NIfTI images is described. This method uses the LWT, SLT, BSVD, and Arnold Cat map. The method was evaluated by employing several NIfTI slices ( $630 \times 630$ ) with a grayscale watermark ( $128 \times 128$ ). Before the watermark was added to the original slice, the ACM was used purposefully to encode it, which was then included in the slice. Thus, nothing can be deduced, even if an unauthorized individual recovers the watermark. It eliminates a typical risk related to using a public watermarking system. The modified watermark is then inserted into the singular value matrix. The results of our approach beat similar watermarking approaches in terms of invisibility and robustness. To watermark the NIfTI images, we choose an arbitrary slice from the NIfTI image containing less medical information from the numerous slices. The suggested approach may insert a watermark in several slices of an NIfTI image. Thus, the suggested watermarking method might authenticate and identify the correct NIfTI picture before diagnosis. After the watermarking, if someone jumbled the slices of the watermarked NIfTI image, recognizing the watermarked slice will be difficult. Each slice needs to be examined to extract the watermark in this scenario, which takes time. It is the downside of our proposed scheme. In subsequent research, we intend to look at this matter further.

We manually chose a slice from the NIfTI image for watermark insertion on the basis of the less-medical-information-containing slice. It is a weak point in the proposed scheme. In the future, it can be improved using some techniques that identify the less informative slice from the NIfTI image.

**Author Contributions:** K.U.S. and A.K. carried out the conception and design. T.A. carried out the analysis and interpretation of the results. T.S. and T.A. and K.U.S. implemented the methodology and performed the computations. All authors have read and agreed to the published version of the manuscript.

**Funding:** The authors have no specific funding for this study.

**Institutional Review Board Statement:** Not applicable.

**Informed Consent Statement:** Not applicable.

**Data Availability Statement:** NIfTI images used in this study were taken from an open database available at <https://zenodo.org/record/3757476#.X0pwCnkzZPZ>, accessed on 23 December 2022.

**Conflicts of Interest:** The authors declare that there are no conflict of interest.

## Abbreviations

The following abbreviations are used in this manuscript:

ACM	Arnold Cat Map
ANALYZE	ANALYZE 7.5
BSVD	Bidiagonal Singular Value Decomposition
CT	Computed Tomography
DCT	Discrete Cosine Transform
DFT	Discrete Fourier Transform
DICOM	Digital Imaging and Communications in Medicine
DWT	Discrete Wavelet Transform
FWT	Fast Walsh Transform
HD	Hessenberg Decomposition
ISLT	Inverse Slantlet Transform
IWT	Integer Wavelet Transform
JPEG	Joint Photographic Experts Group
LWT	Lifting Wavelet Transform
MINC	Medical Imaging NetCDF
MRI	Magnetic Resonance Imaging

NC	Normalized Correlation
NIFTI	Neuroimaging Informatics Technology Initiative
NRRD	Nearly Raw Raster Data
PSNR	Peak Signal-to-Noise Ratio
RSVD	Randomized-Singular Value Decomposition
SLT	Slantlet Transform
SSIM	Structural Similarity Index Metric
SVD	Singular Value Decomposition

## References

- Kumar, A.; Singh, K.U.; Kumar, V.D.A.; Kant, T.; Saudagar, A.K.J.; Al Tameem, A.; Al Khathami, M.; Khan, M.B.; Hasanat, M.H.A.; Malik, K.M. Robust Watermarking Scheme for NIFTI Medical Images. *Comput. Mater. Contin.* **2022**, *71*, 3107–3125. [[CrossRef](#)]
- Singh, K.U.; Abu-Hamatta, H.S.; Kumar, A.; Singhal, A.; Rashid, M.; Bashir, A.K. Secure Watermarking Scheme for Color DICOM Images in Telemedicine Applications. *Comput. Mater. Contin.* **2022**, *70*, 2525–2542. [[CrossRef](#)]
- Singh, K.U.; Singhal, A. Channelized Noise Augmentation to Endorse DICOM Medical Image for Diagnosing. *J. Adv. Res. Dyn. Control. Syst.* **2018**, *10*, 2228–2247.
- Singh, P.; Devi, K.J.; Thakkar, H.K.; Kotecha, K. Region-Based Hybrid Medical Image Watermarking Scheme for Robust and Secured Transmission in IoMT. *IEEE Access* **2022**, *10*, 8974–8993. [[CrossRef](#)]
- Krishnamoorthi, N.; Chinnababu, V.K. Hash and Prediction-Error-Based Reversible Watermarking for Medical Images. *Fluct. Noise Lett.* **2022**, *21*, 2250007. [[CrossRef](#)]
- Salim, M.Z.; Abboud, A.J.; Yildirim, R. A Visual Cryptography-Based Watermarking Approach for the Detection and Localization of Image Forgery. *Electronics* **2022**, *11*, 136. [[CrossRef](#)]
- Meng, X.; Li, J.; Di, X.; Sheng, Y.; Jiang, D. An Encryption Algorithm for Region of Interest in Medical DICOM Based on One-Dimensional e $\lambda$ -cos-cot Map. *Entropy* **2022**, *24*, 901. [[CrossRef](#)]
- Man, Z.; Li, J.; Di, X. Medical image encryption scheme based on self-verification matrix. *IET Image Process.* **2021**, *15*, 2787–2798. [[CrossRef](#)]
- Zhou, J.; Li, J.; Di, X. A Novel Lossless Medical Image Encryption Scheme Based on Game Theory with Optimized ROI Parameters and Hidden ROI Position. *IEEE Access* **2020**, *8*, 122210–122228. [[CrossRef](#)]
- AlShaikh, M. A novel tamper detection watermarking approach for improving image integrity. *Multimed. Tools Appl.* **2022**, *82*, 10039–10060. [[CrossRef](#)]
- Anand, A.; Singh, A.K. Hybrid Nature-Inspired Optimization and Encryption-Based Watermarking for E-Healthcare. *IEEE Trans. Comput. Soc. Syst.* **2022**. [[CrossRef](#)]
- Anand, A.; Singh, A. A method for authenticating digital records for healthcare systems. *Sustain. Comput. Inform. Syst.* **2022**, *33*, 100621. [[CrossRef](#)]
- Gupta, M.K.; Dadheech, P.; Kumar, A.; Dogiwal, S.R.; Poonia, R.C.; Raja, L.; Bhatt, D.P. Detection and localization for watermarking technique using LSB encryption for DICOM Image. *J. Discret. Math. Sci. Cryptogr.* **2022**, *25*, 193–204. [[CrossRef](#)]
- Mashat, A.; Bhatia, S.; Kumar, A.; Dadheech, P.; Alabdali, A. Medical Image Transmission Using Novel Crypto-Compression Scheme. *Intell. Autom. Soft Comput.* **2022**, *32*, 841–857. [[CrossRef](#)]
- Hamidi, M.; El Haziti, M.; Cherifi, H.; El Hassouni, M. Hybrid blind robust image watermarking technique based on DFT-DCT and Arnold transform. *Multimed. Tools Appl.* **2018**, *77*, 27181–27214. [[CrossRef](#)]
- Khare, P.; Srivastava, V.K. Secure and Robust Image Watermarking Scheme Using Homomorphic Transform, SVD and Arnold Transform in RDWT Domain. *Adv. Electr. Electron. Eng.* **2019**, *17*, 343–351. [[CrossRef](#)]
- Sun, L.; Xu, J.; Liu, S.; Zhang, S.; Li, Y.; Shen, C. A robust image watermarking scheme using Arnold transform and BP neural network. *Neural Comput. Appl.* **2018**, *30*, 2425–2440. [[CrossRef](#)]
- Zhou, N.R.; Hou, W.M.X.; Wen, R.H.; Zou, W.P. Imperceptible digital watermarking scheme in multiple transform domains. *Multimed. Tools Appl.* **2018**, *77*, 30251–30267. [[CrossRef](#)]
- Chang, C.; Shen, J. Features classification forest: A novel development that is adaptable to robust blind watermarking techniques. *IEEE Trans. Image Process.* **2017**, *26*, 3921–3935. [[CrossRef](#)]
- Singh, S.; Bhatnagar, G. A new robust watermarking system in integer DCT domain. *J. Vis. Commun. Image Represent.* **2018**, *53*, 86–101. [[CrossRef](#)]
- Kang, X.B.; Zhao, F.; Lin, G.F.; Chen, Y.J. A novel hybrid of DCT and SVD in DWT domain for robust and invisible blind image watermarking with optimal embedding strength. *Multimed. Tools Appl.* **2018**, *77*, 13197–13224. [[CrossRef](#)]
- Hsu, L.; Hu, H. Robust blind image watermarking using crisscross inter-block prediction in the DCT domain. *J. Vis. Commun. Image Represent.* **2017**, *46*, 33–47. [[CrossRef](#)]
- Singh, D.; Singh, S.K. DWT-SVD and DCT based robust and blind watermarking scheme for copyright protection. *Multimed. Tools Appl.* **2017**, *76*, 13001–13024. [[CrossRef](#)]
- Rayachoti, E.; Tirumalasetty, S.; Prathipati, S.C. SLT based watermarking system for secure telemedicine. *Clust. Comput.* **2020**, *23*, 3175–3184. [[CrossRef](#)]

25. Thabit, R.; Khoo, B.E. Medical image authentication using SLT and IWT schemes. *Multimed. Tools Appl.* **2015**, *76*, 309–332. [[CrossRef](#)]
26. Bamal, R.; Kasana, S.S. Dual hybrid medical watermarking using walsh-slantlet transform. *Multimed. Tools Appl.* **2019**, *78*, 17899–17927. [[CrossRef](#)]
27. Jayashree, N.; Bhuvaneshwaran, R.S. A Robust Image Watermarking Scheme Using Z-Transform, Discrete Wavelet Transform and Bidiagonal Singular Value Decomposition. *Comput. Mater. Contin.* **2019**, *58*, 263–285. [[CrossRef](#)]
28. Assini, I.; Hassan II University Casablanca; Badri, A.; Safi, K.; Sahel, A.; Baghdad, A. A Robust Hybrid Watermarking Technique for Securing Medical Image. *Int. J. Intell. Eng. Syst.* **2018**, *11*, 169–176. [[CrossRef](#)]
29. Zermi, N.; Khaldi, A.; Kafi, R.; Kahlessenane, F.; Euschi, S. A DWT-SVD based robust digital watermarking for medical image security. *Forensic Sci. Int.* **2021**, *320*, 110691. [[CrossRef](#)]
30. Singh, K.U.; Kumar, A.; Singh, T.; Ram, M. Image-based decision making for reliable and proper diagnosing in NIFTI format using watermarking. *Multimed. Tools Appl.* **2022**, *81*, 39577–39603. [[CrossRef](#)]
31. Bhatnagar, G.; Raman, B. Robust reference-watermarking scheme using wavelet packet transform and bidiagonal-singular value decomposition. *Int. J. Image Graph.* **2009**, *9*, 449–477. [[CrossRef](#)]
32. Selesnick, I.W. The slantlet transform. *IEEE Trans. Signal Process.* **1999**, *47*, 1304–1313. [[CrossRef](#)]
33. Sweldens, W. The Lifting Scheme: A Construction of Second Generation Wavelets. *SIAM J. Math. Anal.* **1998**, *29*, 511–546. [[CrossRef](#)]
34. Sweldens, W. The Lifting Scheme: A Custom-Design Construction of Biorthogonal Wavelets. *Appl. Comput. Harmon. Anal.* **1996**, *3*, 186–200. [[CrossRef](#)]
35. Wang, K.; Gao, T.; You, D.; Wu, X.; Kan, H. A secure dual-color image watermarking scheme based 2D DWT, SVD and Chaotic map. *Multimed. Tools Appl.* **2022**, *81*, 6159–6190. [[CrossRef](#)]
36. Singh, K.U.; Hsieh, S.Y.; Swarup, C.; Singh, T. Authentication of NifTI Neuroimages Using Lifting Wavelet Transform, Arnold Cat Map, Z-Transform, and Hessenberg Decomposition. *Traitement Signal* **2022**, *39*, 265–274. [[CrossRef](#)]
37. Ma, J.; Ge, C.; Wang, Y.; An, X.; Gao, J.; Yu, Z.; Zhang, M.; Liu, X.; Deng, X.; Cao, S.; et al. COVID-19 CT lung and infection segmentation dataset. 2020. [[CrossRef](#)]
38. Singh, K.U.; Kumar, A.; Singh, T. Authentication of Lung CT-Scan Data in NifTI Format Using LWT, Hessenberg Decomposition, and Affine Transform. *IETE J. Res.* **2023**. [[CrossRef](#)]

**Disclaimer/Publisher’s Note:** The statements, opinions and data contained in all publications are solely those of the individual author(s) and contributor(s) and not of MDPI and/or the editor(s). MDPI and/or the editor(s) disclaim responsibility for any injury to people or property resulting from any ideas, methods, instructions or products referred to in the content.